**Atmospheric
Chemistry
and Physics**

Heterogeneous OH oxidation of palmitic acid in single component and internally mixed aerosol particles: vaporization and the role of particle phase

V. F. McNeill[1,2]**, R. L. N. Yatavelli**[1]**, J. A. Thornton**[1]**, C. B. Stipe**[3]**, and O. Landgrebe**[1]

[1]Department of Atmospheric Sciences, University of Washington, Seattle, Washington, 98195, USA
[2]Department of Chemical Engineering, Columbia University, New York, New York, 10027, USA
[3]Department of Mechanical Engineering, Seattle University, Seattle, Washington, 98122, USA

Abstract. We studied the OH oxidation of submicron aerosol particles consisting of pure palmitic acid (PA) or thin (near monolayer) coatings of PA on aqueous and effloresced inorganic salt particles. Experiments were performed as a function of particle size and OH exposure using a continuous-flow photochemical reaction chamber coupled to a chemical ionization mass spectrometer (CIMS) system, for detection of gas and particle-bound organics, and a DMA/CPC for monitoring particle size distributions. The loss rate of PA observed for pure PA aerosols and PA on crystalline NaCl aerosols indicates that the OH oxidation of PA at the gas-aerosol interface is efficient. The pure PA oxidation data are well represented by a model consisting of four main processes: 1) surface-only reactions between OH and palmitic acid, 2) secondary reactions between palmitic acid and OH oxidation products, 3) volatilization of condensed-phase mass, and 4) a surface renewal process. Using this model we infer a value of γ^{OH} between 0.8 and 1. The oxidation of palmitic acid in thin film coatings of salt particles is also efficient, though the inferred γ^{OH} is lower, ranging from ∼0.3 (+0.1/−0.05) for coatings on solid NaCl and ∼0.05 (±0.01) on aqueous NaCl particles. These results, together with simultaneous data on particle size change and volatilized oxidation products, provide support for the ideas that oxidative aging of aliphatic organic aerosol is a source of small oxidized volatile organic compounds (OVOCs), and that OH oxidation may initiate secondary condensed-phase reactions.

1 Introduction

Atmospheric aerosols impact Earth's radiation balance both directly by scattering solar radiation and indirectly via cloud properties (Forster et al., 2007), and they influence atmospheric composition via heterogeneous and multiphase chemistry (Jacob, 2000; Liao and Seinfeld, 2005). Organic matter typically comprises 10 to 90% of tropospheric fine aerosol mass (Kanakidou et al., 2005). Recently, this prevalence and importance has renewed interest in the sources and sinks of aerosol organic matter, with heterogeneous aging by atmospheric oxidants gaining significant attention (Rudich et al., 2007). One motivation has been to characterize the timescale and mechanisms for converting the aerosol material from hydrophobic to hydrophilic via oxidation. Such a conversion may alter both the radiative properties of the aerosol, by increasing water uptake, and their cloud droplet nucleating ability. Heterogeneous oxidation also has the potential to induce volatilization of condensed-phase material via radical decomposition, which would lead to reduced particle mass and would serve as a source of oxidized volatile organic compounds (OVOCs) (Molina et al., 2004).

Particle phase and morphology have been observed to affect the aging process, and also to change with aging, mainly in the case of O_3 oxidation (Knopf et al., 2005; Hearn and Smith, 2005; Katrib et al., 2005; Hearn and Smith, 2007). While OH oxidation has been much less studied in this regard, it has also been observed to induce changes in particle density (George et al., 2007). Heterogeneous oxidation could convert solid organic particles into more liquid-like particles by increasing the number of components and functionality (Marcolli et al., 2004). Gas-phase oxidants will undergo slow diffusion in a solid organic matrix or in viscous liquids such
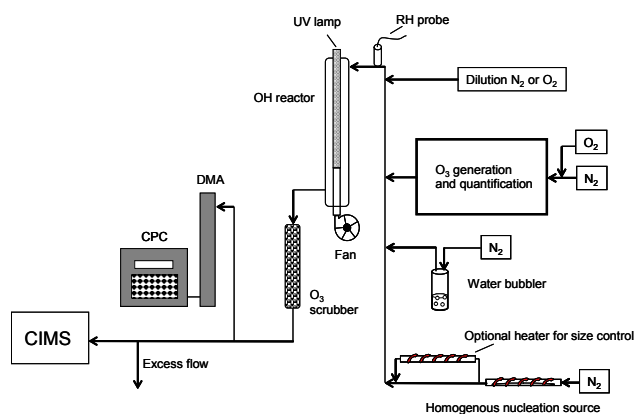
Fig. 1. Schematic of the experimental set-up

as those that are supercooled or structured (Hearn and Smith, 2005; Katrib et al., 2005; Knopf et al., 2005). Therefore, the reactive zone for OH oxidation, which is expected to be fast (Bertram et al., 2001; Molina et al., 2004; Lambe et al., 2007; George et al., 2007), may be confined to the particle surface or near-surface region (Hanson et al., 1994; Worsnop et al., 2002) leading to differences in the transformation rates between the surface and bulk (Maria et al., 2004). To our knowledge, this aspect has not been thoroughly examined by laboratory studies.

Recent studies offer conflicting evidence as to the prevalence of secondary condensed-phase chemistry and also mass loss by volatilization initiated by heterogeneous oxidation. Molina et al. (2004) showed that OH oxidation of self-assembled monolayers (SAMs) led to the volatilization of about 6–9 carbons per OH collision. Hearn et al. (2007) used a relative rates technique to study Cl-initiated oxidation of liquid bis(2-ethylhexyl) sebacate (BES) particles and found that the reaction probability, $\gamma^{Cl} \sim 2$. They concluded that a reaction probability exceeding unity implied the existence of radical-assisted secondary chemistry occuring in the particle bulk. In contrast, George and coworkers used the aerosol flow tube technique to study the oxidation of liquid BES particles with OH in the absence of NO_x (George et al., 2007). They observed very efficient oxidation (γ^{OH} 1.3±0.4) but no strong indication of secondary chemistry. From the observed particle size and density changes, and condensed phase product information, George et al. (2007) concluded that the predominant fate of the organic peroxy radical product (RO_2) was self reaction to form condensed-phase carbonyl and alcohol products. Alkoxy radical formation and subsequent volatilization due to decomposition was found to be a minor reaction pathway. The same group used PTR-MS to measure VOC yields from the OH oxidation of BES, soot, stearic acid, and pyrene films (Vlasenko et al., 2008). They observed a variety of volatile oxidation products, including formic acid. They found that VOC yield varied for the different film types, with stearic acid showing the most significant

volatilization. Lambe et al. (2007) studied the OH oxidation of hexacosane, which is a solid at room temperature, in an aerosol chamber with AMS detection. They report efficient oxidation, with γ^{OH}=1.04±0.21 and report volatilization and secondary chemistry to be minor. It is clear that substantial uncertainty remains as to the potential for heterogeneous oxidation to initiate secondary chemistry and volatilization, and how these processes might depend on particle morphologies or composition.

We present a laboratory investigation of the OH oxidation of pure palmitic acid aerosols and palmitic acid present as a thin (near monolayer) film on NaCl particles. One motivation of this study was to extend the investigations of OH oxidation to particles with different compositions, using the same experimental technique, for direct comparion of reactivity differences. By using palmitic acid in surface films and pure particles we tried to span the regimes examined in separate studies using SAMs or single component particles. The results from both sets of our experiments, while showing some differences, are consistent with efficient oxidation occurring at the particle surface, and provide evidence for secondary condensed-phase chemistry, especially in the pure particle case. Evidence also exists for volatilization of oxidation products in the observed particle size changes and low-molecular weight species detected by mass spectrometry upon OH exposure. The data are represented well by a model that assumes palmitic acid reacts with OH and oxidation products, these reactions occur only at the particle surface, a process exists (i.e. volatilization) to renew the particle surface with palmitic acid from the bulk, and particle mass loss due to volatilization occurs at a rate proportional to the palmitic acid loss rate.

2 Experimental

Experiments were performed using a continuous flow photochemical reaction chamber coupled to a chemical ionization mass spectrometer (CIMS) system. Volatilization and detection of organics in the particle phase was achieved using a heated inlet for thermal desorption. A differential mobility analyzer/condensation particle counter (DMA/CPC, Grimm Technologies) was used for measuring aerosol size distributions. The setup is similar to that described in McNeill, et al. (2007), but we provide a summary and important differences below. Figure 1 shows a schematic of the apparatus.

2.1 Aerosol generation and characterization

Pure palmitic acid aerosols were generated via homogeneous nucleation as described in Thornton et al. (2003). A 30 cm long, 13 mm O.D. Pyrex tube was loaded with pure palmitic acid crystals and wrapped in heating tape, and a thermocouple measured the external temperature of the tube. A temperature controller (Omega) was used to maintain the

particle source at 95–115°C. Particles were entrained in a flow of 500 sccm dry N_2. Mean particle size was controlled by changing the source temperature and/or the bulk flow rate. In some experiments, smaller sizes were achieved by passing the source effluent through a second empty heated tube which served to partially evaporate and denude excess palmitic acid. The resulting aerosol stream was mixed with 2 slpm N_2 carrier gas. The carrier gas was humidified to approximately 16% RH for OH generation (see below). In some experiments, an additional stream of 500 sccm O_2 was also added and the N_2 carrier flow was reduced, to simulate a 20% O_2 atmosphere in the reactor.

Palmitic acid-coated NaCl particles were made via vapor deposition of palmitic acid onto crystallized salt particles following Kwamena et al. (2004). NaCl particles were generated by a constant output atomizer (TSI) operating with a 0.05 M solution of NaCl in deionized water. A 1 slpm portion of the atomizer output passed through a diffusion drier before entering the palmitic acid source to insure the submicron NaCl particles were effloresced. For coating, the temperature of the palmitic acid source (described above) was maintained at 70–80°C. At the exit of the palmitic acid source, the coated particles were mixed with ∼1.5 slpm N_2 carrier flow. For the experiments performed on solid salt particles, the carrier gas was humidified to approximately 16% RH for OH generation, but the aerosol stream was not further humidified before entering the photochemical reaction chamber. NaCl aerosol crystallize at 43% RH and deliquesce at RH ∼75% (Cziczo et al., 1997; Tang et al., 1997), thus we assume the aerosol remained crystalline during OH exposure under these conditions. For the experiments involving aqueous aerosols, the aerosol stream was passed through an in-line humidifier to raise the RH above the deliquescence point (RH≥80% for NaCl) before entering the reactor. The humidifier was 20 cm long and consisted of 6 mm OD permeable Teflon tubing (Zeus, Inc.) housed inside a 13 mm O.D. stainless steel tube. The space between the steel and Teflon tubes was filled with deionized water. The steel tube was wrapped with heating tape (VWR), and the external temperature was maintained at 40°C using a temperature controller and a thermocouple. After exiting the humidifier, the aerosol stream was passed through a 3 m, 13 mm OD PFA tube to allow ∼12 s equilibration with water vapor before entering the reactor. The RH of the equilibrated N_2/aerosol stream was monitored at the inlet to the reaction chamber with a hygrometer (Vaisala).

Aerosol size distributions were continuously obtained by a DMA and CPC in series, which in most experiments sampled the particle stream exiting the photocell. This configuration was chosen to provide a better measure of reactor aerosol concentrations, since small mass losses were associated with particles impacting as they passed through a 90° bend at the reactor entrance. The coated aerosol populations exhibited a near log-normal size distribution not distinguishable from that of the pure salt particle population, with a typical geometric standard deviation of 2.0. The coated aerosols had a typical mean surface-weighted particle radius r_p∼120 nm, and total aerosol surface area was typically between 4×10^{-4}–1×10^{-3} cm^2 cm^{-3}. Typical volume-weighted particle radii for the pure palmitic acid aerosols were varied from 85–220 nm, with a typical geometric standard deviation of 1.25.

2.2 Continuous flow photocell reactor

The reactor consisted of a quartz photocell 25 cm long and 5 cm in diameter with a 1 cm inner sleeve containing an ozone-free Hg pen-ray lamp (Jelight, 254 nm). OH was formed from the reaction of $O(^1D)$ with water, where $O(^1D)$ is produced by ozone photolysis. O_3 was generated continuously during experiments by flowing a mixture of O_2 and N_2 through a photocell containing a Hg pen-ray lamp (UVP) operating at 185 nm. The O_3 concentration of the outlet stream was monitored using a UV absorption cell equipped with another Hg pen-ray lamp (Jelight) coated to primarily emit 254 nm, a 254 nm interference filter, and a photodiode (Thorlabs). The desired O_3 concentration was achieved by adjusting the relative concentrations of O_2 and N_2. The RH-equilibrated aerosol stream was mixed with the O_3/N_2/O_2 mixture at the entrance to the photocell reactor. The initial concentration of O_3 in the photocell ranged from 0.2–25 ppm. O_2 mixing ratios were varied from ∼2%–20%. Additional experiments were performed in which O_2 was maintained at 20% across a range of OH exposures in order to elucidate any effects of O_2 on particle chemistry.

OH concentrations in the photoreactor were inferred via calibration experiments using the observed loss of SO_2 and the recommended rate constant for the reaction of SO_2 with OH (DeMore et al., 1997). Sample cylinders of 50 ppm SO_2 in N_2 were prepared from a pure SO_2 cylinder (Matheson), and 5–10 sccm of this mixture was diluted in 1.4–1.6 slpm humidified N_2 in order to create 4.5–7.5×10^{12} molec cm^{-3} SO_2 and 16% RH in the flow tube. The loss of SO_2 in the presence of UV light was monitored by CIMS as a function of initial O_3 concentration. The observed loss was compared to the output of a photochemical model that includes ozone photolysis to yield $O(^1D)$ and its reaction with H_2O, as well as several HO_x cycling reactions, HO_x self-reactions, a diffusion-limited loss of OH on the reactor walls, and a loss of OH on particles. The latter process was disabled when comparing to SO_2 titrations which were performed in the absence of particles. The observed SO_2 reactivity was used to constrain only two parameters: the photolytic rate constant for O_3 and the diffusion-limited rate constant for OH loss at the reactor walls. Adjusting the O_3 photolytic rate constant alone was sufficient to give reasonably good agreement between model and data. Including the OH wall loss parameter improved the model's ability to reproduce the curvature in the observed SO_2 loss (and thus OH concentration) versus O_3 mixing ratio. The model, which will be published as supplemental information, was
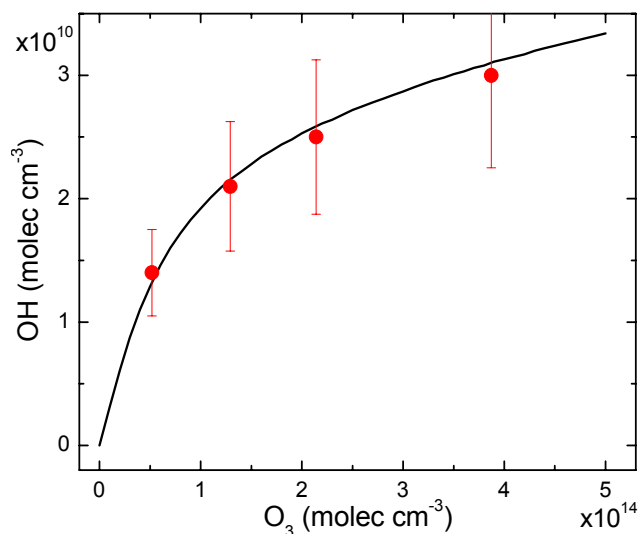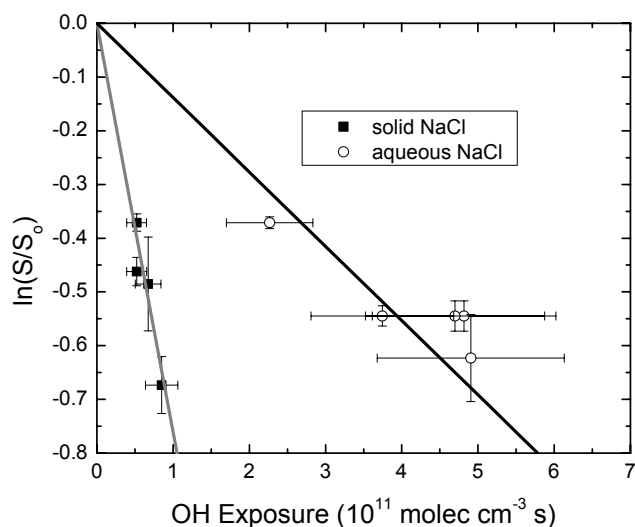
Fig. 2. OH predicted by the photochemical box model (line) compared to that calculated from SO_2 loss experiments (circles). Error bars represent 25% uncertainty in OH calibration data.

Fig. 3. Loss of palmitic acid on dry (squares) and aqueous (circles) NaCl particles as a function of OH exposure. Lines represent the error-weighted linear least squares fits to the experimental data. RH for aqueous experiments is >80%.

then used to predict reactor OH concentrations and PA loss simultaneously for a given O_3 concentration and exposure time. Figure 2 shows the OH predicted by the model and that inferred from the SO_2 loss in the reactor as a function of the initial O_3 mixing ratio.

2.3 CIMS detection of reactants and products

The chemical ionization mass spectrometer (CIMS) system and the detection method for organic acids has been described in detail previously (McNeill et al., 2006, 2007). Palmitic acid and its OH-oxidation products containing a carboxylic acid functionality are detected with $I^- \cdot (H_2O)$ as the reagent ion undergoing ligand-switching reactions. For example, palmitic acid was monitored as the cluster with $I^-(I^- \cdot C_{16}H_{32}O_2)$ at 383 amu. In this study, organics in the particle phase were volatilized for detection by thermal desorption in a continuous flow heated inlet (Hearn and Smith, 2004; McNeill et al., 2007). For comparison purposes, in a few experiments with PA-coated NaCl particles, we used a novel impactor coupled to the CIMS inlet currently under development in our group. Particles are collected on a surface that is subsequently heated. Similar kinetics and products were observed with both detection methods.

Detection of the components occurred at the exit of a 23 cm long, 1.27 cm O.D. PFA tube wrapped with heating tape (VWR). This inlet's temperature was monitored and controlled using a thermocouple and temperature controller (Omega). The response of the signal to varying pure particle aerosol mass concentration or the coated particle aerosol surface area was linear, with a sensitivity of 268 ± 34 Hz $\mu g^{-1} m^3$. Based on various calibrations we sus-

pect all carboxylic acids are theoretically detected with a similar sensitivity, to within a factor of 2, for a given water vapor concentration, but no attempt was made to calibrate to invidual products and thus absolute product yields are not derived. SO_2 was detected using SF_6^- and a reduced chemical ionization reaction time to minimize the effect of O_3. Ozone reacts with SF_6^-, but at a slower rate than SO_2. In addition, high water vapor conditions were also precluded when using SF_6^-.

Experiments were conducted by first aquiring an initial mass spectrometer signal for the given particle and O_3 concentrations, in the absence of UV light. The lamp was then turned on, causing a decrease in the palmitic acid signal and an increase in signals at masses corresponding to oxidation products. Background signals in the absence of particles were measured at the beginning and end of each experiment. To obtain mechanistic information, O_3 concentrations and/or reactor residence time (and thus OH concentration and exposure) were varied. Depending on the experiment, total flow rate varied from 1.7 to 3 slpm, corresponding to a residence time in the photocell of 10 to 17 s. For all experiments except volatile product studies and the SO_2 calibration of the photoreactor, the reactor effluent was passed through a diffusion tube packed with Carulite O_3-scrubbing catalyst (Caruschem) before entering the heated CIMS inlet.
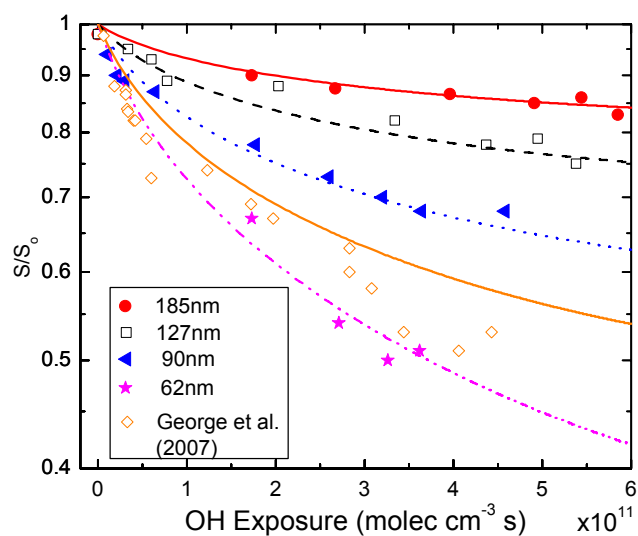
Fig. 4. Palmitic acid remaining for pure particles of four different sizes, 185 nm (●), 127 nm (□), 90 nm (◀), and 62 nm (⋆) versus OH exposure. Data shown as diamonds are those of George, et al. (2007). Symbols represent experimental data and the lines represent model predictions for the respective sizes.

Fig. 5. Relative change in initial radius for pure palmitic acid particles of two different sizes, 160 nm (O), and 90 nm (◀). Symbols represent experimental data and the lines represent model predictions for the respective sizes.
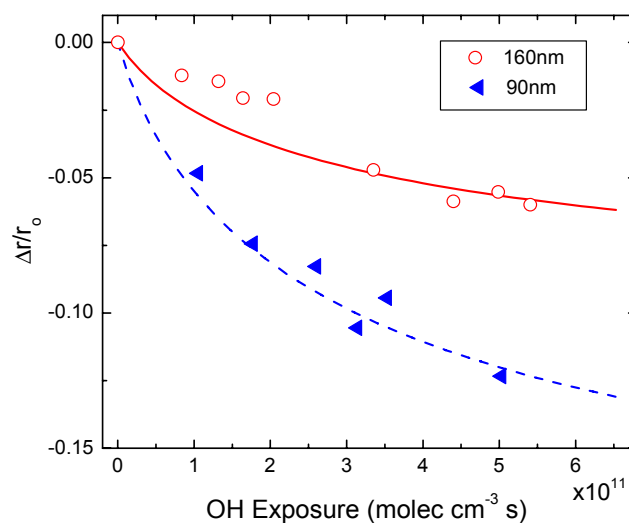
3 Results

3.1 Kinetics of palmitic acid film oxidation

For both solid and aqueous NaCl particles, we observed a prompt decrease in palmitic acid signal when the UV lamp was turned on in the presence of O_3 and H_2O. The OH concentration and residence time in the flow tube were varied to examine the extent of loss as a function of OH exposure ([OH]×t). Due to experimental limitations on flow ratios, only a small range in OH exposure could be examined for each aerosol type. Figure 3 shows palmitic acid loss data for the coated particles. The fraction of PA remaining relative to the baseline PA signal is shown on a log scale as a function of OH exposure. Loss data are shown for solid particles (squares) and particles equilibrated at RH >80% which we assume are aqueous (circles). A substantial difference exists in the OH oxidation kinetics of PA on solid and aqueous particles, with PA on solid NaCl particles exhibiting greater loss at lower OH exposure than observed for PA on aqueous particles.

Assuming a heterogeneous reaction between OH and PA at the surface of the coated particles, the loss rate of PA can be expressed as:

$$\frac{d[PA]_{surf}}{dt} = -k^{II}[OH][PA]_{surf} \qquad (1)$$

where k^{II} is the second-order rate coefficient, and $[PA]_{surf}$ is the surface concentration of palmitic acid, in molec cm^{-2}. A plot of the natural log of the ratio of PA signal at each OH exposure to the PA signal in the absence of OH, S/S_0, is fit

reasonably well with a straight line forced through the origin ($R^2 \sim$ 0.86–0.96). S/S_0 is proportional to $[PA]_{surf} / [PA]_{surf,0}$ since the surface area to mass ratio for these particles is constant (in the case of the coated particles) or nearly so (for pure PA particles). The slope of the error-weighted linear least-squares fit yields the observed pseudo-first-order rate coefficient, $k^I = k^{II}[OH]$, which is then related to the reaction probability for an encounter between OH (g) and PA (s) in the free molecular regime, γ^{OH} according to:

$$\gamma^{OH} = \frac{4k^I}{\sigma_{PA}\omega_{OH}} \qquad (2)$$

where σ_{PA} is the molecular cross-section of PA at the surface and ω_{OH} is the thermal velocity of OH. In this study we assume $\sigma_{PA} \sim 2 \times 10^{-15}$ cm^2/molec based on Langmuir trough measurements of palmitic acid films on water (Adam, 1921). Applying this equation and correcting for the effects of gas-phase diffusion and transition regime effects for Kn $\sim$1 (Fuchs and Sutugin, 1970) yields reaction probabilities of $\gamma^{OH} \sim$0.05±0.01 for PA on aqueous particles and $\gamma^{OH} \sim$0.3 +0.1/-0.05 for PA on solid salt particles. The reported uncertainty stems from propagating a ±25% uncertainty in OH concentrations through equation (2) and the transition regime correction. These reaction probabilities assume that the PA signal arising from these coated particles is largely determined by surface area; thus, the surface-weighted particle radius was used to determine the transition regime correction.

3.2   Kinetics of pure Palmitic Acid Particle oxidation

In Fig. 4, the fraction of PA remaining relative to the baseline PA signal, S/S_0, is shown on a log scale as a function of OH exposure for four different initial mean volume weighted particle sizes: r_0=62 nm, 90 nm, 127 nm, and 185 nm. For all sizes the PA signal decreases with increasing exposure. The relative loss increases as mean size decreases. This behavior is consistent with a gas-surface mechanism, since the surface area-to-volume ratio increases with decreasing particle size. The signal ratio in both log and linear space is nonlinear with OH exposure. This nonlinearity is most evident in the small particle data, though it is clear that psuedo-first order kinetics is not appropriate for the larger sizes either. With no mechanism to refresh the surface, the loss rate of condensed-phase PA due to heterogeneous oxidation is expected to slow with increased OH exposure due to the decreased probability of OH reacting with PA upon collision with the particle (Ammann, et al., 2003). However, the deceleration appears to be more prompt for PA particles than for liquid BES particles (George et al., 2007). For comparison, we have included the BES oxidation data from George, et al. (2007) shown as diamonds. In addition to the observed nonlinearity, far more PA is lost than would be present at the surface, and thus PA originally below the surface layer is reacting with OH. That is, OH is penetrating into the bulk of the particle, or sub-surface layers are being exposed to OH.

Figure 5 shows the relative change in particle radius as a function of OH exposure for pure PA particles with initial mean volume weighted particle radii r_0=160 nm and 90 nm. After an OH exposure of $\sim 3 \times 10^{11}$ molec cm^{-3} s, the absolute change in radius was $\sim$9 nm and 6.4 nm for the initial radii of 90 nm and 160 nm, respectively.

3.3   Oxidation products

Mass spectra were taken in the presence and abscence of both OH and particles in order to examine the types of products generated during OH oxidation. In an attempt to account for species that might be produced from OH reaction on the flow tube walls or from the fragmentation of PA itself, we took three different types of spectra: 1) OH and PA particles present, 2) OH present but no PA particles, 3) no OH but PA particles present. Figure 6 shows the result of subtracting spectra types 2 and 3 from spectrum type 1. Peaks corresponding to species with both lower and higher molecular weights than PA remain positive in this difference spectrum. The exception is a peak at 399 amu, which appeared when PA particles were exposed to O_3 only but increased above this baseline with OH (see Fig. 7). Most notable in this difference spectrum is the dominant peak corresponding to formic acid, $I^- \cdot (HCOOH)$, located at 173 amu, and the envelope of peaks between 200–300 amu (see inset) that correspond to oxidation products with molecular weights lower than that of PA. Our ion chemistry is largely specific to com-

pounds containing carboxylic acid groups, i.e. aldehydes or ketones are not detected unless a carboxylic acid moeity is present.

To approximately evaluate the gas-particle partitioning of the oxidation products, spectra were also taken during oxidation, but without thermal desorption at the inlet. All oxidation products detected at masses below $\sim$300 amu were also observed in the absence of heating, that is, they were likely gas-phase products. Notable particle-bound products (i.e. those observed only during thermal desorption) include those detected at 397.2 amu and 399.2 amu (14 amu and 16 amu higher than the palmitic acid signal, respectively). Figure 7 shows the development of these particle-bound product signals with OH exposure. These product signals have been corrected for background signals in the absence of OH.

4   Analysis and interpretation

In the following section, we give a brief interpretation of the OH oxidation kinetics of palmitic acid coatings on salt particles and then connect this data to the kinetics of pure palmitic acid particle oxidation. The uncertainty in our OH exposure coordinate in both cases is likely the largest contributor to the total uncertainty of our measurements. Our SO_2 titrations, essentially a relative rate experiment, provided [OH]×t estimates that were reproducible to within $\sim$25%. This level of uncertainty has a fairly substantial effect on the derived reaction probabilities, in part because of the nonlinearity in the diffusion correction as the measured reaction probability increases. Additional uncertainties stem from using the model to predict OH at RH greater than those of the SO_2 titration experiments. This issue is especially important for the PA coatings on aqueous salt particles. Thus, we have much more confidence in our pure palmitc acid oxidation experiments and the PA coated dry salt experiments, but we feel able to conclude that the observed difference between kinetics on solid and aqueous particles is significant.

4.1   Palmitic acid oxidation on solid and aqueous particles

We infer a reaction probability, γ^{OH}, of $\sim$0.3+0.1/−0.05 for palmitic acid molecules on the surface of crystalline salt particles. This value is in general agreement with the lower limit of 0.2 determined by Bertram, et al. (2001) using a flow tube with paraffin wax-coated walls. To our knowledge, our data are the first to examine the reactivity of OH with surface-bound palmitic acid on submicron salt particles.

It is clear from Fig. 3 that the oxidation of PA in aqueous salt particles is slower by a factor of $\sim$5 or more than on solid particles. Even though significant uncertainty exists in the OH exposure at high RH because we were unable to calibrate for OH at 89% RH, it seems unlikely that the inferred OH is too high by a factor of five. At this time, we
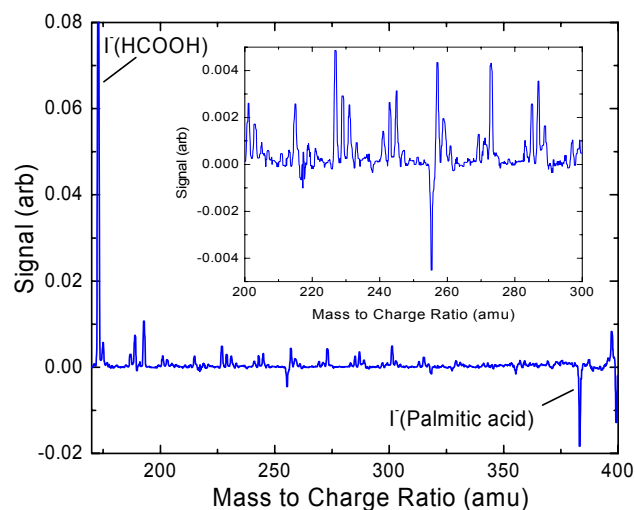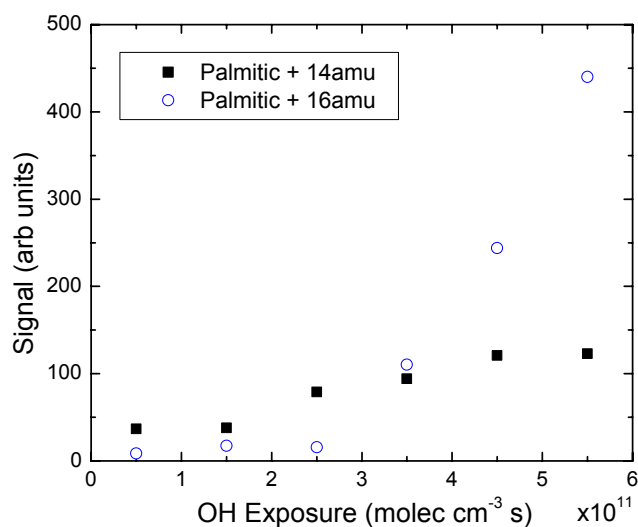
Fig. 6. Mass spectra showing smaller-molecular-weight products from palmitic acid oxidation by OH. Inset is the magnification of the spectrum from 200 to 300 m/z.

Fig. 7. Plot showing two palmitic acid products in particle phase, palmitic acid + 14 amu (keto-acid, ■), and PA + 16 amu (hydroxy acid, O), for an OH exposure of 4.7×10^{11} molec s cm^{-3}.

can only speculate as to the reasons for this difference. On the one hand, the PA in aqueous particles may not be distributed entirely at the surface but exist in phase-separated agglomerates not easily accessed by OH. In this case, our model represented by equations 1 and 2 is invalid. On the other hand, we have indirect evidence from the inefficient hydrolysis of N_2O_5 on these PA-coated aqueous particles that would suggest a significant coating of PA at the surface (McNeill et al., 2006, 2007). If PA is at the surface of these aqueous salt particles, a possible explanation for the reduced efficiency of OH oxidation might be due to the orientation of PA relative to the gas-phase. PA, a surface-active fatty acid, may orient itself at the gas-aerosol interface in an inverted micelle configuration, in which case the attacking OH would most likely collide with a primary carbon at the end of the hydrocarbon tail (Myers, 2006; Gill et al., 1983; Ellison et al., 1999). Hydrogen extraction from a primary carbon is much less efficient than secondary or tertiary carbons in the gas-phase; for OH reacting with ethane in the gas phase, the bimolecular rate constant at ∼300 K is 2.74×10^{-13} cm^3 molec^{-1} s^{-1}, while for OH + n-butane, it is ∼2.76×10^{-12} cm^3 molec^{-1} s^{-1} (Atkinson, 1986). Perhaps a similar effect is present in gas-surface reactions. Nevertheless, the data shown here are, to our knowledge, the first of their kind. More work is needed before it will be possible to draw strong conclusions about the effects of particle phase and surface morphology on the OH oxidation efficiency of surface-bound organics.

4.2 Oxidation of pure palmitic acid particles

We presume, as have others, that the initial steps in the mechanism of particle-phase OH oxidation are analogous to gas-

phase hydrogen atom abstraction (Molina et al., 2004; Eliason et al., 2004; George et al., 2007). Given the levels of O_2 in our reactor, the likely result of OH reacting with a surface-bound PA is O_2 addition to the alkyl radical forming an organic peroxy radical (RO_2). We saw no dependence on O_2 concentration for the range used in our experiments. The fate of this RO_2 could be reaction with HO_2 to form organic hydroperoxides (ROOH), or self-reaction to either yield stable hydroxy and carbonyl products or an alkoxy (RO) radical. The alkoxy radical can then isomerize and react with O_2 to form a hydroxyperoxy radical. Alternatively, the RO can react with O_2 to form a stable carbonyl product or undergo bond scission to yield smaller molecular weight fragments. This latter path is the most likely to lead to mass loss by volatilization. Recently, secondary condensed-phase chemistry between the radical oxidation products and the primary particle component has been proposed to explain Cl radical – BES reaction probabilities that exceed unity (Hearn et al., 2007). If secondary chemistry occurs, it is likely to occur via the higher energy alkoxy radical than RO_2.

Our observation of volatile, lower-molecular-weight products from the OH oxidation of palmitic acid is qualitatively consistent with Molina et al. (2004), who observed OH-initiated volatilization of SAMs and macroscopic solid organic surfaces, and with the stearic acid oxidation studies of Vlasenko et al. (2008). We also previously observed gas-phase products upon exposure of thin films of oleate to OH (McNeill et al., 2007). Our observations of the reactor effluent composition and the decrease in mobility diameter with OH exposure suggest mass loss by volatilization, consistent with a mechanism that includes alkoxy radical formation followed by bond scission. Both scission and non-scission OH
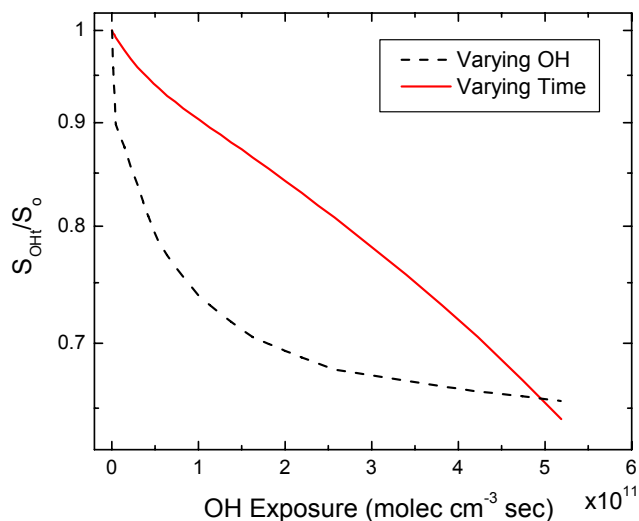
Fig. 8. Model results for palmitic acid remaining versus OH exposure calculated using two different methods, varying OH concentration with constant reaction time (dashed line), and varying reaction time keeping OH constant (solid line)

oxidation products might additionally undergo further oxidation partly via the scission pathway. George et al. (2007) and Hearn and Smith (2007) observed that ketone and alcohols were the dominant products for BES oxidation. While some volatilization was inferred through particle size changes in the study by George et al. (2007), no direct observation of lower-molecular-weight gas-phase species were made in either of these studies. As shown in Fig. 7, except for the highest OH exposures, our inferred ketoacid oxidation product species at 397.2 amu was present in greater abundance than the hydroxyacid at 399.2 amu. This suggests that alkyl peroxy radical self-reaction to form a carbonyl and alcohol is not the dominant reaction pathway in this system at low OH exposures. See, for example, pathway (2) in George, et al. (2007).

The OH oxidation of palmitic acid in single component particles occurs well beyond the initial surface layer given that one monolayer on a 125 nm radius particle accounts for ~5% by mole of the particle content. Given the high reactivity of OH with aliphatic compounds, its reacto-diffusive length will be very short in a liquid particle, ~1 nm, and even shorter if the particle is a solid (due to a higher resistance to diffusion in the solid). Thus, the observed extent of oxidation is not expected unless there is some mechanism to refresh the surface (i.e. volatilization) or to propogate the oxidation into the bulk (i.e. secondary condensed phase radical chemistry). An alternative explanation is that the palmitic acid particles exist as a supercooled liquid, i.e. that the surface is refreshed via mixing within the particle and/or OH can undergo substantial diffusion into the particle. However, a model based on reactive uptake of OH to a liquid particle, that includes the assumption that every OH colliding with the particle surface

would encounter the initial particle component (Worsnop et al., 2002), does not reproduce the majority of our data well.

We developed a numerical model in order to interpret our results in the context of a fast surface reaction, secondary condensed phase chemistry, and mass loss by volatilization. The unique aspects of this model are that it assumes palmitic acid reacts with OH only at the particle surface and it requires no *a priori* assumptions about particle phase or instantaneous mixing. Processes included are: 1) the reaction of OH with PA at the surface, 2) secondary reactions between oxidation products and unreacted PA, and 3) a surface renewal process which exposes fresh PA to the surface. In addition, we allow particle size to change in the model for comparison to observed electric mobility size changes during oxidation..

The differential equation governing the fractional surface coverage of PA (θ_{PA}) is:

$$\frac{d\theta_{PA}}{dt} = -k_1 [OH]\theta_{PA} - k_2 (1-\theta_{PA})\,\theta_{PA} + k_{ren} (1-\theta_{PA}) \qquad (3)$$

where k_1 is related to k^I described in Eq. (2) in that $k^I = k_1[OH]$ in the free-molecular regime. We account for transition regime effects in the calculation of k_1, and k_2 is the second-order rate constant for secondary reactions between PA and oxidation products in the surface layer. The surface concentration of products is simply $1-\theta_{PA}$. We assume the total number of surface sites does not change over the course of an experiment. The renewal of the surface is taken to be first order in the surface concentration of products, with a rate constant k_{ren}. Possible physical interpretations of this renewal process include the volatilzation of products which in turn exposes underlying PA, or a liquification of the surface layer into which subsurface PA would dissolve and OH would diffuse.

The relevant quantity for comparing model output to the experimental results is the fraction of PA remaining after exposure ($n_{PA}/n_{PA,0}$):

$$\frac{d\left(n_{PA}/n_{PA,0}\right)}{dt} = \frac{1}{n_{PA,0}}\frac{3}{r\sigma}\left(-k_1 [OH]\,\theta_{PA} - k_2 (1-\theta_{PA})\,\theta_{PA}\right) \qquad (4)$$

Note that vaporization of the oxidation products does not directly reduce the total PA concentration in the particle. Particle size change due to vaporization is calculated according to

$$\frac{dr}{dt} = \chi_{vap}\frac{r_0^3}{3r^2}\frac{d\left(n_{PA}/n_{PA,0}\right)}{dt} \qquad (5)$$

where r_0 is the initial particle radius, and χ_{vap} is a factor meant to relate the combined effects of density changes and mass loss by volatilization to the rate of palmitic acid oxidation (Katrib et al., 2005; George et al., 2007). Equations (3)–(5) and those governing the production and destruction of OH are solved simultaneously with a fixed integration time equal to the photoreactor residence time. Inputs to the model are

RH, O_3, particle surface area, and volume-weighted r_p. Initially, the surface is assumed to consist of palmitic acid only (θ_{PA}=1). The model is compared to the observed palmitic acid loss, and γ^{OH}, k_2, k_{ren}, and χ_{vap} are adjusted to minimize the model-measurement difference.

Model simulations are shown as lines in Figs. 4 and 5. Both the PA loss observed for all particle sizes with the CIMS and the observed mobility size change can be simulated well with a single set of parameters: γ^{OH}=1, k_2=0.22 s^{-1}, k_{ren}=0.35 s^{-1}, and χ_{vap}=0.9. At short OH exposures, the model is most sensitive to the choice of γ^{OH} and k_2. A value of γ^{OH}<1 can be used, but must be compensated for by increasing k_2. This compensation works only within a narrow range of γ^{OH}. For example, setting γ^{OH}=0.5 and k_2=0.4 s^{-1} can grossly reproduce the data but the modeled curvature is too steep at low OH exposures and too shallow at high OH exposures. At larger OH exposures, the surface renewal process becomes rate-limiting. The PA loss observed with the CIMS is fairly insensitive to the value of χ_{vap}, which can range from ∼0.75–1 without significant loss of agreement. This parameter controls the rate of particle size change, and while a decrease in size does accelerate the oxidation of the surface by decreasing the gas-phase diffusion limitation, the relative size change is not large enough to compete with the surface renewal term except in the smallest sizes examined (r_p∼60 nm). The mobility size change data, however, are very sensitive to χ_{vap}, and require χ_{vap}∼0.9.

For comparison, we applied our model to the data of George, et al. (2007) using only their reported initial volume-weighted radius. As shown in Fig. 4, the model consistently underestimates their observed extent of reaction for the same model parameters that best match our data. A larger surface renewal term and a slightly larger secondary chemistry term are required to match the George, et al. (2007) data. We attribute these differences to the likelihood that PA particles are solids while BES particles are liquids. Therefore, in BES particles OH will have a greater reacto-diffusive length and the surface may be refreshed by mixing within the particle.

Laboratory studies of atmospheric heterogeneous chemistry face a challenge when aiming for close replication of atmospheric conditions given the very low oxidant levels (sub pptv) and long interaction times (days to weeks). The exposure coordinate is used to analyze kinetics under the assumption that the product of oxidant concentration and interaction time allows for the direct comparison of low-concentration and long-time conditions with high-concentration and short-time conditions. In Fig. 8, we show the results from two different versions of our model described above. In one simulation, we fixed the OH concentration while vaying the interaction time over which the rate equations were integrated. In the other simulation, we fixed the integration time over which the rate equations were integrated while varying the OH concentration. The implication is that, at least for the reaction mechanism in our model, the exposure coordinate may not allow direct extrapolation to atmospheric conditions. By

systematically eliminating various processes from the model we find that it is the combination of surface renewal and secondary chemistry that gives rise to the difference in model output along the OH exposure coordinate for the two scenarios.

4.3 Physical interpretation of model parameters

The combined mass spectral and mobility size data suggest that for pure palmitic acid particles γ^{OH} is likely between 0.8 and 1. This value is in general agreement with other studies using single component organic aerosols, organic films, and SAMs (Bertram et al., 2001; Molina et al., 2004; Lambe et al., 2007; George et al., 2007). Using the same apparatus, we measure a smaller reaction probability for thin palmitic acid films (γ^{OH}∼0.3). Given the challenges of this particular experiment and the uncertainty in the OH exposure, we refrain from inferring too much from this difference; for example, if the uncorrected γ^{OH} was 0.5, instead of 0.3, the diffusion correction would lead to a γ^{OH}=1.

For the best agreement between our model and the pure palmitic acid data, a non-zero rate constant is required for the reaction of surface-bound palmitic acid with reaction products. Our model could be improved by speciating the oxidation products into RO_2 and RO radicals, but the scatter in the present data set doesn't provide a strong test of more complicated pathways. The main point is that our data support the existence of secondary condensed-phase chemistry, and our model suggests a fairly simple mechanism that could explain observations of reaction probabilities exceeding unity (Hearn et al., 2007). In our model, the rate of secondary reactions between OH oxidation products and PA at the surface is at a maximum when $\theta_{PA} \ll 1$ and a psuedo-first order rate constant then approaches the value of k_2=0.22 s^{-1}. This rate constant can be compared to the diffusion-limited rate constant for OH oxidation of PA at the surface, a typical value being ∼0.45 s^{-1} for [OH] ∼3×10^{10} molec cm^{-3} and r_p=150 nm. Thus, while reaction with OH is the dominant fate of surface PA, secondary chemistry can account for as much as 10–30% of surface PA loss depending on the exact OH collision frequency in our reactor.

Formation and photolysis of organic hydroperoxides (ROOH) is one possible mechanism that could explain our inference of secondary particle-phase chemistry which enhances palmitic acid loss. ROOH would form from the reaction of surface-bound RO_2 with HO_2. Subsequent loss of ROOH by photolysis at 254 nm would lead to the formation of RO and OH radicals in the condensed phase, adding to the pool of radicals formed by other pathways. The net effect of this chemistry would be to enhance the oxidation rate of palmitic acid and the branching to alkoxy radicals. The latter would enhance the degree of volatilization per collision of gaseous OH with the particle surface. We note that this chemistry is would possibly be important only in our experimental setup, and that of George et al. (2007), but not in

the atmosphere. It is important to note that neither we, nor George et al. detected ROOH products in the particle phase.

Our evaluation of this chemistry demonstrates that it may well be occurring, but that it doesn't impact our main conclusions: namely, $\gamma^{OH} > 0.8$ on pure palmitic acid particles, and mass loss by volatilization due to heterogeneous OH oxidation is unlikely to be important in the atmosphere (see below). To evaluate the potential importance of this pathway, we incorporated RO_2 and ROOH formation and loss into our surface-chemistry model. Due to the lack of available information about necessary parameters, we attempt to provide an upper-limit estimate by assuming that every HO_2 collision with an RO_2 at the surface produces an ROOH, and that the photolysis of each ROOH leads to the oxidation of a palmitic acid molecule. We assume the photolysis frequency of ROOH is the same as for CH_3OOH, which we calculate relative to our calibrated ozone photolysis frequency using the ratio of CH_3OOH and O_3 absorption cross sections at 254 nm (De More et al., 1997). We also ran a simulation with the ROOH photolysis frequency a factor of 100 larger than this value. We do not allow for any other secondary loss processes of palmitic acid. Under these circumstances, the model generally reproduces the observed palmitic acid decay, especially at the higher OH exposures, but continues to underestimate palmitic acid loss at low OH exposures. We require $\gamma^{OH} \sim 1$–1.4 to simulate the palmitic acid loss, with the values above unity suggesting that not all loss processes have been identified. Thus, ROOH chemistry, as we have modeled here, can explain a significant fraction of the inferred secondary chemistry required in the simpler model, but this chemistry does not affect the large γ^{OH} inferred for this system.

A surface renewal process is needed to explain our observation that more PA is oxidized than is initially present in the surface layer. If we assume this renewal process is driven by volatilization, then our parameterization suggests that essentially two oxidation events of a PA molecule leads to volatilzation and the exposure of a new palmtic acid at the surface. This conclusion is based on the value of k_{ren} being similar to the typical psuedo-first order rate coefficient for OH striking a surface-bound PA ($\sim 0.45\,\text{s}^{-1}$) and that the renewal rate scales with the coverage of oxidation products. Molina et al. (2004) found using SAMs that roughly 6–9 carbons were volatilized per OH collision. For palmitic acid, if one OH reaction event were to volatilize 6 carbons, the first event would lead to an oxidized C_{10} product that may be of low enough volatility to remain in the particle phase. Reaction of this C_{10} product would lead to a C_4 and a C_6 product, both potentially volatile. Thus, our results seem roughly consistent with this level of volatilization by OH oxidation of PA. We expand on this issue below. An alternative to volatilization as the renewal process is liquification of the surface layer upon oxidation, which would be thermodynamically expected (Marcolli et al., 2004). This liquification would provide a means for bulk PA to migrate rapidly to the

surface and/or for OH to diffuse more rapidly into the subsurface region. The fact that we observe low molecular weight products and a decrease in electrical mobility diameter supports volatilization as a viable surface renewal process.

To best reproduce the observed decrease in electrical mobility diameter, the radius must change essentially at the same rate as PA, i.e. $\chi_{vap} \sim 0.9$. Given that the bulk palmitic acid loss rate in the model is largely controlled by the surface renewal process, the observed decrease in size also suggests volatilization. An implication of the radius change being tied to the PA oxidation rate is that the rate of volatilization is not constant with OH exposure, i.e. aging. Indeed, our results suggest that the particle size should eventually stop changing with very high OH exposures. We infer that the oxidized material that remains in the particle phase becomes less likely to volatilize upon collision with OH. If volatilization is tied only to the oxidation of a PA molecule, and the surface renewal process is via liquification, then experiments to supress the surface renewal rate, for example, cooling the particle stream, should yield smaller decreases in particle size for the same OH exposures used here.

Electrical mobility diameter depends on other factors such as particle shape, which is also likely changing if the pure palmitic particles initially have a rough crystalline morphology that becomes smoothed by oxidation or liquification. Taking all the results together, however, we feel it reasonable to conclude that particle mass loss by volatilization initially occurs with an effeciency similar to that observed by Molina, et al. (2004) leading to an overall decrease in the size of pure palmitic acid particles upon OH exposure, but that the efficiency of volatilization per OH collision decreases exponentially with OH exposure such that this process would likely become unimportant in the atmosphere as an organic aerosol mass loss. In addition, ROOH production and subsequent photolysis would enhance the flux through alkoxy radicals, and thus enhance the potential for volatilazation by RO decomposition. Above, we estimate that ROOH chemistry may be occuring in our system to an extent that is greater than would occur in the atmosphere, and thus some fraction of the observed volatilization could be due to these unrealistic conditions which would further limit the actual importance of volatilization as an organic aerosol mass loss.

5 Summary and atmospheric implications

The loss rate of PA in the particle phase, as observed for pure PA aerosols and PA-coated solid NaCl aerosols, indicates that the OH oxidation of PA at the gas-aerosol interface is efficient, with γ^{OH} ranging from 0.3 for thin palmitic acid films on solid substrates to ~ 1 for pure palmitic acid particles. Interestingly, for thin palmitic acid films on aqueous substrates we infer a substantially lower γ^{OH} of ~ 0.05 implying that mophology of the organic surface may impact the OH oxidation rate.

For all aerosol types studied, many of the observed oxidation products were volatile at 298 K. We observed a reduction in volume-weighted mean particle diameter of up to 12% for 90 nm palmitic acid particles, which corresponds to a maximum volume loss of ~30% after an equivalent 6 days of OH processing in the atmosphere. The kinetics and particle size change data for OH oxidation of pure PA aerosols are well-represented by a model consisting of surface-only reactions with volatilization of products, surface renewal, and secondary chemistry between PA and oxidation products. These results suggest that alkoxy radical formation followed by bond scission to produce low-molecular weight products is active in this system with an efficiency similar to the lower end of that observed by Molina, et al. (2004). This pathway can be a potentially important source of OVOCs in the upper troposphere, as well as a potentially important sink for organic aerosol mass. The initial mass loss rates observed in this study, which utilized highly aliphatic particles, are consistent with estimates by Kwan et al. (2006) that organic aerosol oxidation may result in OVOC fluxes of up to 70 pptv C/day. However, the importance of this pathway appears to depend on oxidant type, particle type (Knopf et al., 2006; George et al., 2007; Hearn et al., 2007; Vlasenko et al., 2008), and particle age as implied by our results. As such, it is unlikely that a persistent 70 pptv C/day OVOC source exists in the upper troposphere and unlikely that mass loss by volatilization will compete significantly as a control on overall particle lifetime.

In comparing our data to studies utilizing liquid particles, we observe, consistent with our expectations, that the heterogeneous oxidation rate of organic aerosol mass is fastest for material residing at the surface, rather than the bulk. This gradient in oxidation rates is steeper for particles that are solid, such as palmitic acid particles used here, compared to those that are liquids. Atmospheric aerosol particles are certainly complex mixtures of multiple components, and it is possible some particles are more solid, structured or otherwise diffusion-resistant than others. Likewise, liquid particles may undergo phase transitions in the colder upper troposphere which could affect their chemistry (Hearn and Smith, 2005, 2007). These issues may preclude the use of a single constant reaction probability in models, and the sensitivity of predicted organic aerosol loadings and OVOC concentrations to these effects should be assessed.

Finally, we show that hypothetical experiments which vary interaction time while keeping [OH] constant may exhibit different oxidation kinetics from those which vary [OH] while keeping the interaction time constant. The differences in the model output for the two experiment types are due to surface renewal and secondary chemistry processes, with implications for experiment designs or comparisons between different data sets along the OH exposure coordinate.

References

Adam, N. K.: The properties and molecular structure of thin films of palmitic acid on water. Part I, Proc. Roy. Soc. London A, 99, 336–351, 1921.

Ammann, M., Poschl, U., and Rudich, Y.: Effects of reversible adsorption and Langmuir-Hinshelwood surface reactions on gas uptake by atmospheric particles, Phys. Chem. Chem. Phys., 5, 351–356, 2003.

Atkinson, R.: Kinetics and mechanisms of the gas-phase reactions of the hydroxyl radical with organic compounds under atmospheric conditions, Chem. Rev., 86, 69–201, 1986.

Bertram, A. K., Ivanov, A. V., Hunter, M., Molina, L. T., and Molina, M. J.: The reaction probability of OH on organic surfaces of tropospheric interest, J. Phys. Chem. A, 105, 9415–9421, 2001.

Cziczo, D. J., Nowak, J. B., Hu, J. H., and Abbatt, J. P. D.: Infrared spectroscopy of model tropospheric aerosols as a function of relative humidity: Observation of deliquescence and crystallization, J. Geophys. Res.-Atmos., 102, 18 843–18 850, 1997.

DeMore, W. B., Sander, S. P., Golden, D. M., Hampson, R. F., Kurylo, M. J., Howard, C. J., Ravishankara, A. R., Kolb, C. E., and Molina, M. J.: Chemical kinetics and photochemical data for use in stratospheric modeling, National Aeronautics and Space Administration Jet Propulsion Laboratory, Pasadena, CA, USA, 1997.

Eliason, T. L., Gilman, J. B., and Vaida, V.: Oxidation of organic films relevant to atmospheric aerosols, Atmos. Environ., 38, 1367–1378, 2004.

Ellison, G. B., Tuck, A. F., and Vaida, V.: Atmospheric processing of organic aerosols, J. Geophys. Res.-Atmos., 104, 11 633–11 641, 1999.

Forster, P., Ramaswamy, V., Artaxo, P., Berntsen, T., Betts, R., Fahey, D. W., Haywood, J., Lean, J., Lowe, D. C., Myhre, G., Nganga, J., Prinn, R., Raga, G., Schulz, M., and Van Dorland, R.: Changes in atmospheric constituents and in Radiative Forcing, in: Climate Change 2007: The Physical Science Basis. Contribution of Working Group I to the Fourth Assessment Report of the Intergovernmental Panel on Climate Change, edited by: Solomon, S., Qin, D., Manning, M., Chen, Z., Marquis, M., Averyt, K. B., Tignor, M., and Miller, H. L., Cambridge University Press, Cambridge, UK and New York, NY, USA, 2007.

Fuchs, N. A. and Sutugin, A. G.: Highly Dispersed Aerosols, Ann Arbor Science Pulishers, Ann Arbor, 47–59, 1970.

George, I. J., Vlasenko, A., Slowik, J. G., Broekhuizen, K., and Abbatt, J. P. D.: Heterogeneous oxidation of saturated organic aerosols by hydroxyl radicals: Uptake kinetics, condensed-phase products, and particle size change, Atmos. Chem. Phys., 7, 4187–4201, 2007,
http://www.atmos-chem-phys.net/7/4187/2007/.

Gill, P. S., Graedel, T. E., and Weschler, C. J.: Organic films on atmospheric aerosol-particles, fog droplets, cloud droplets, rain-drops, and snowflakes, Rev. Geophys., 21, 903–920, 1983.

Hanson, D. R., Ravishankara, A. R., and Solomon, S.: Heterogeneous reactions in sulfuric-acid aerosols – A framework for model calculations, J. Geophys. Res.-Atmos., 99, 3615–3629, 1994.

Hearn, J. D., Renbaum, L. H., Wang, X., and Smith, G. D.: Kinetics and products from a reaction of Cl radicals with dioctyl sebacate (DOS) particles in O_2: a model for radical-initiated oxidation of organic aerosols, Phys. Chem. Chem. Phys., 9, 1–11, 2007.

Hearn, J. D. and Smith, G. D.: A chemical ionization mass spectrometry method for the online analysis of organic aerosols, Anal. Chem., 76, 2820–2826, 2004.

Hearn, J. D. and Smith, G. D.: Measuring rates of reaction in supercooled organic particles with implications for atmospheric aerosol, Phys. Chem. Chem. Phys., 7, 2549–2551, 2005.

Hearn, J. D. and Smith, G. D.: Ozonolysis of mixed oleic acid/n-docosane particles: The roles of phase, morphology, and metastable states, J. Phys. Chem. A, 111, 11 059–11 065, 2007.

Jacob, D. J.: Heterogeneous chemistry and tropospheric ozone, Atmos. Environ., 34, 2131–2159, 2000.

Kanakidou, M., Seinfeld, J. H., Pandis, S. N., Barnes, I., Dentener, F. J., Facchini, M. C., Van Dingenen, R., Ervens, B., Nenes, A., Nielsen, C. J., Swietlicki, E., Putaud, J. P., Balkanski, Y., Fuzzi, S., Horth, J., Moortgat, G. K., Winterhalter, R., Myhre, C. E. L., Tsigaridis, K., Vignati, E., Stephanou, E. G., and Wilson, J.: Organic aerosol and global climate modelling: A review, Atmos. Chem. Phys., 5, 1053–1123, 2005,
http://www.atmos-chem-phys.net/5/1053/2005/.

Katrib, Y., Biskos, G., Buseck, P. R., Davidovits, P., Jayne, J. T., Mochida, M., Wise, M. E., Worsnop, D. R., and Martin, S. T.: Ozonolysis of mixed oleic-acid/stearic-acid particles: Reaction kinetics and chemical morphology, J. Phys. Chem. A, 109, 10 910–10 919, 2005.

Knopf, D. A., Anthony, L. M., and Bertram, A. K.: Reactive uptake of O_3 by multicomponent and multiphase mixtures containing oleic acid, J. Phys. Chem. A, 109, 5579–5589, 2005.

Knopf, D. A., Mak, J., Gross, S., and Bertram, A. K.: Does atmospheric processing of saturated hydrocarbon surfaces by NO_3 lead to volatilization?, Geophys. Res. Lett., 33, L17816, doi:10.1029/2006GL026884, 2006.

Kwamena, N. O. A., Thornton, J. A., and Abbatt, J. P. D.: Kinetics of surface-bound benzo[a]pyrene and ozone on solid organic and salt aerosols, J. Phys. Chem. A, 108, 11 626–11 634, 2004.

Kwan, A. J., Crounse, J. D., Clarke, A. D., Shinozuka, Y., Anderson, B. E., Crawford, J. H., Avery, M. A., McNaughton, C. S., Brune, W. H., Singh, H. B., and Wennberg, P. O.: On the flux of oxygenated volatile organic compounds from organic aerosol oxidation, Geophys. Res. Lett., 33, L15815, doi:10.1029/2006GL026144, 2006.

Lambe, A. T., Zhang, J. Y., Sage, A. M., and Donahue, N. M.: Controlled OH radical production via ozone-alkene reactions for use in aerosol aging studies, Environ. Sci. Technol., 41, 2357–2363, 2007.

Liao, H. and Seinfeld, J. H.: Global impacts of gas-phase chemistry-aerosol interactions on direct radiative forcing by anthropogenic aerosols and ozone, J. Geophys. Res.-Atmos., 110, doi:10.1029/2005JD005907, 2005.

Marcolli, C., Luo, B. P., and Peter, T.: Mixing of the organic aerosol fractions: Liquids as the thermodynamically stable phases, J. Phys. Chem. A, 108, 2216–2224, 2004.

Maria, S. F., Russell, L. M., Gilles, M. K., and Myneni, S. C. B.: Organic aerosol growth mechanisms and their climate-forcing implications, Science, 306, 1921–1924, 2004.

McNeil, V. F., Wolfe, G. M., and Thornton, J. A.: The oxidation of oleate in submicron aqueous salt aerosols: Evidence of a surface process, J. Phys. Chem. A., 111, 1073–1083, 2007.

McNeill, V. F., Patterson, J., Wolfe, G. M., and Thornton, J. A.: The effect of varying levels of surfactant on the reactive uptake of N_2O_5 to aqueous aerosol, Atmos. Chem. Phys., 6, 1635–1644, 2006,
http://www.atmos-chem-phys.net/6/1635/2006/.

Molina, M. J., Ivanov, A. V., Trakhtenberg, S., and Molina, L. T.: Atmospheric evolution of organic aerosol, Geophys. Res. Lett., 31, L22104, doi:10.1029/2004GL020910, 2004.

Myers, D.: Surfactant science and technology, John Wiley and Sons, Hoboken, NJ, USA, 107–157, 2006.

Rudich, Y., Donahue, N. M., and Mentel, T. F.: Aging of organic aerosol: Bridging the gap between laboratory and field studies, Annu. Rev. Phys. Chem., 58, 321–352, 2007.

Tang, I. N., Tridico, A. C., and Fung, K. H.: Thermodynamic and optical properties of sea salt aerosols, J. Geophys. Res.-Atmos., 102, 23 269–23 275, 1997.

Thornton, J. A., Braban, C. F., and Abbatt, J. P. D.: N_2O_5 hydrolysis on sub-micron organic aerosols: the effect of relative humidity, particle phase, and particle size, Phys. Chem. Chem. Phys., 5, 4593–4603, 2003.

Worsnop, D. R., Morris, J. W., Shi, Q., Davidovits, P., and Kolb, C. E.: A chemical kinetic model for reactive transformations of aerosol particles, Geophys. Res. Lett., 20, p. 1996, doi:10.1029/2002GL015542, 2002.

Vlasenko, A. George, I. J., and Abbatt, J. P. D.: Formation of volatile organic compounds in the heterogeneous oxidation of condensed-phase organic films by gas-phase OH, J. Phys. Chem. A, ASAP Article, 112, doi:10.1021/jp0772979, 1552–1560, 2008.